Signatures of the superfluid–to–Mott-insulator transition in cold bosonic atoms in a one-dimensional optical lattice

S. Ramanan*
Centre for High Energy Physics, Indian Institute of Science, Bangalore 560 012, India

Tapan Mishra† and Meetu Sethi Luthra‡
Indian Institute of Astrophysics, II Block, Kormangala, Bangalore 560 034, India

Ramesh V. Pai§
Department of Physics, Goa University, Taleigao Plateau, Goa 403 206, India

B. P. Das‖
Indian Institute of Astrophysics, II Block, Kormangala, Bangalore 560 034, India
(Received 20 November 2008; published 27 January 2009)

We study the Bose-Hubbard model using the finite size density matrix renormalization group method. We obtain a complete phase diagram for a system in the presence of a harmonic trap and compare it with that of the homogeneous system. The superfluid to the Mott-insulator phase transition is investigated using different experimental signatures of these phases in quantities such as momentum distribution, visibility, condensate fraction, and the total number of bosons at a particular density. The relationships between the various experimental signatures and the phase diagram are highlighted.

DOI: 10.1103/PhysRevA.79.013625 PACS number(s): 03.75.Nt, 05.10.Cc, 05.30.Jp

I. INTRODUCTION

In recent years many theoretical and experimental investigations have been carried out in the field of ultracold atoms in optical lattices [1–3]. The interest in bosonic systems began with the seminal paper by Fisher *et al.* [4], where a phase transition from a superfluid (SF) to a Mott insulator (MI) in a lattice of bosons was predicted when the on-site Coulomb repulsion between the atoms dominates the nearest neighbor hopping amplitude. Since then, a variety of theoretical approaches [5–15] have been used to study the Bose-Hubbard model (BHM) [4]. There is good agreement between the phase diagrams obtained from the different techniques. While the BHM was originally developed in the context of ^{4}He [4], its potential to describe ultracold bosons trapped in an optical lattice was soon realized by Jaksch *et al.* [16]. This paper has had a great impact on the condensed matter community because high-precision experiments on cold atoms in traps can now be used as a powerful and reliable tool to study a variety of quantum phase transitions [1–3]. The experimental realization of the quantum phase transition from the superfluid to the Mott insulator in three dimensions [17], two dimensions [18], as well as in one dimension [19] soon followed. The bosons in an optical lattice are well described by the Bose-Hubbard model modified to include a trap potential [16], which is normally harmonic. In the presence of a trap, the density profile exhibits a rich structure as the SF and the MI phases coexist. A variety of numerical methods have been applied to understand the model [20–26]. The most important aspect that has emerged is the lack of a global phase in these systems. As an analogy, in three dimensions the superfluid and the Mott-insulator phases coexist as shells in an onion. The unprecedented control over the system parameters by tuning the laser intensity has paved the path for the experimental realization of these predictions [27,28].

In this paper, we revisit the one-dimensional Bose-Hubbard model using the density matrix renormalization group method. Our main motivation is to obtain the phase diagram, given the experimental realization of the shell structure and their signatures. The Bose-Hubbard model, describing bosons in an optical lattice, is given by

$$H = -t\sum_{\langle i,j\rangle}(a_i^\dagger a_j + \text{H.c.}) + \frac{U}{2}\sum_i n_i(n_i-1) + V_t\sum_i r_i^2 n_i, \quad (1)$$

where t is the hopping amplitude, U is the on-site repulsion between the atoms, V_t is the depth of the external trapping potential, $a_i^\dagger$ (a_i) is the bosonic creation (annihilation) operator, $n_i = a_i^\dagger a_i$ is the number operator, and r_i is the position of the ith lattice site from the trap center. For simplicity, the energy is scaled in units of the hopping amplitude, which is set to one. As a result the Hamiltonian and the related observables are dimensionless.

In experiments, the optical lattice potential (V_{OL}), formed by the superposition of three counterpropagating laser beams [2,29], can be written as

$$V_{OL} = V_0[\sin^2(k_L x) + \sin^2(k_L y) + \sin^2(k_L z)], \quad (2)$$

where V_0 is the lattice depth measured in units of the single photon recoil energy E_R, $k_L = 2\pi/\lambda_L$ is the wave vector, and

*suna@cts.iisc.ernet.in
†tapan@iiap.res.in
‡Permanent address: Bhaskaracharya College of Applied Sciences, Phase-I, Sector-2, Dwarka, Delhi 110075, India; sethi.meetu@gmail.com.
§rvpai@unigoa.ac.in
‖das@iiap.res.in

λ_L is the laser wavelength. Increasing the intensity of the beam in two directions restricts the hopping to one dimension and this results in a one-dimensional lattice. The on-site interaction U and the hopping amplitude t are related to V_0 and E_R as follows:

$$\frac{U}{t} \propto \exp(2V_0/E_R)^{1/2}. \tag{3}$$

Therefore, by varying the lattice depth the ratio of U/t can be tuned.

Earlier studies of the homogeneous system show that when the on-site interaction strength U is small compared to the hopping amplitude t, the system remains in the SF phase characterized by long range coherence. When U increases and becomes much larger than t, a transition from the SF to the MI phase occurs at some critical value of $U=U_c\sim 3.4$ (in units of t) [8–10]. This transition belongs to the Kosterlitz-Thouless universality class [30,31]. The SF-MI transition gets more interesting in the presence of a trap [32–35]. In this case, the entire system remains in the SF phase for small U values, but as U increases, a MI phase develops around a central SF phase, followed by a SF shoulder. A further increase in U ultimately results in a MI phase throughout the lattice with the exception of the trap edges, which we refer to as a central MI phase. This alternating occurrence of the SF and the MI phases can be observed in the number density profile. The system exhibits a plateau at integer densities (MI phase) surrounded by a region of noninteger densities (SF phase) [20–26,32–35] and this has been recently observed in experiments [27,28] in three-dimensional (3D) optical lattices.

In this paper, we first obtain the phase diagram of the model, given by Eq. (1), in the homogeneous ($V_t=0$) limit. We then extend our analysis to the inhomogeneous case and compare it with the homogeneous case. Finally, we obtain experimentally measurable quantities such as condensate fraction, visibility, and density profile and deduce the inhomogeneous phase diagram. We also discuss how the shell structure in the optical lattice can be observed from condensate fraction and visibility.

This paper is structured as follows: Sec. II contains a brief discussion on the finite size density matrix renormalization group (FS-DMRG) technique. Section III discusses the phase diagram obtained from the number density profile, while Sec. IV analyzes the experimental signature for the phase transition and we summarize our results in Sec. V.

II. METHOD OF CALCULATION

We have employed the FS-DMRG method [36,37] with an open-boundary condition to determine the ground state energy and the wave function of the system. This method is one of the most powerful techniques in one dimension and has been widely used to study the Bose-Hubbard model [8–10,33,34]. We have considered a soft-core case by retaining four bosonic states per site and the weight of the states neglected in the density matrix formed from the left or right blocks is less than 10^{-6}. For better convergence of the ground state energies of various phases, we have performed a finite size sweeping procedure [9,36], twice in each iteration of the FS-DMRG method.

Our FS-DMRG method consists of two steps: (i) a DMRG iteration where the length of the system L is increased to $L+2$ and (ii) finite size sweeping to achieve better convergence of the ground state energy $E_L(N)$ [9,36]. We consider a system with an initial length $L=4$ and the number of bosons $N=4$. The FS-DMRG procedure is then employed, keeping the density of bosons fixed at $\rho=1$, until we have a desired number of bosons in the system, say $N=30$. Then onward, in the FS-DMRG iteration, only the length of the system is increased keeping N fixed, until the system grows to a desired size, for example, $L=100$. At this point we have a system of length $L=100$ with $N=30$ bosons. Now keeping the length fixed, we increase N in steps of 1 at the end of each FS-DMRG sweep. In our example, N is varied from 30 to 150. Thus at the end of the FS-DMRG calculation, for a given set of parameter values, we have ground state energies $E_L(N)$ and wave functions $|\psi_{LN}\rangle$ for a system of length $L=100$ with N varying from 30 to 150. From $E_L(N)$, we obtain the chemical potential μ of the system

$$\mu = \frac{\delta E_L(N)}{\delta N}. \tag{4}$$

The on-site local number density $\langle n_i\rangle$ is defined as

$$\langle n_i\rangle = \langle \psi_{LN}|n_i|\psi_{LN}\rangle. \tag{5}$$

The compressibility κ for a homogeneous system can be defined as

$$\kappa = \frac{\delta n}{\delta \mu}, \tag{6}$$

where $n=N/L$. The number density is uniform throughout the system except at the edges due to boundary effects. However, for finite V_t the lattice is inhomogeneous and as a result the local density $\langle n_i\rangle$ attains its maximum value at the center of the trap where the potential is minimum and decreases as we move away from the center, eventually going to zero. For this case, the local compressibility is relevant and can be defined as

$$\kappa_i = \frac{\delta n_i}{\delta \mu_i}. \tag{7}$$

In most of our calculations, we have taken $V_t=0.004$ and 0.008, length L up to 200, with N ranging between 30 and 150 and U between 2 and 20.

III. RESULTS AND DISCUSSIONS

A. Homogeneous case

We begin our discussions with the homogeneous case. The density of the system $\langle n\rangle$ as a function of the chemical potential μ for three values of $U=3$, 4, and 7 are shown in the top panels of Fig. 1. The formation of a plateau in the $\langle n\rangle$ versus μ plots, for $U=4$ and 7 at $\langle n\rangle=1$, in contrast to $U=3$, signals the onset of the $\rho=1$ MI phase, where ρ denotes the density per site. The lower panels in Fig. 1 show the

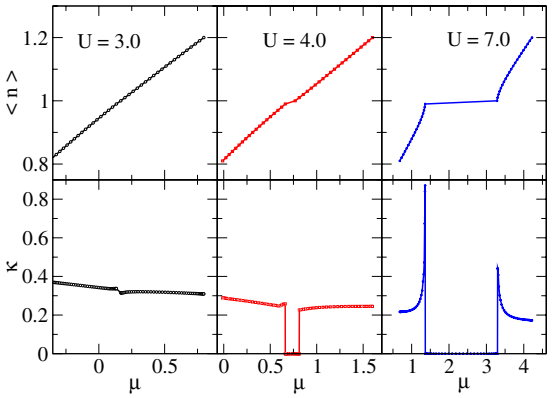

FIG. 1. (Color online) Variation of the compressibility κ (lower panels) and the density $\langle n\rangle$ (upper panels) as a function of μ for the homogeneous case (V_t=0). The plateau region at $\langle n\rangle$=1 and κ=0 signals the incompressible (ρ=1) MI phase.

compressibility κ [calculated using Eq. (6)] as a function of μ. It is clear that the MI phase is incompressible, i.e., κ=0. The cusp in κ as $\langle n\rangle$ approaches 1, shown in Fig. 1, is due to quantum criticality. The phase diagram for the homogeneous system is obtained by picking out the values of μ at the knees where $\langle n\rangle$=1 and κ=0 and plotting them in the μ-U plane. This is shown in Fig. 2 and is in agreement with earlier results [8–10,13]. The cusp in the compressibility reflects the Kosterlitz-Thouless-type behavior of the SF-MI transition.

B. Inhomogeneous case

We now analyze the case when there is a finite trapping potential V_t in the Bose-Hubbard Hamiltonian. Taking the depth of the trap V_t=0.004, the number of bosons N=100, and the length L=200, we obtain the local density profile $\langle n_i\rangle$ as a function of the distance from the center of the trap r_i, as shown in Fig. 3. In contrast to the homogeneous case, $\langle n_i\rangle$ is not uniform when the trap is finite. It decreases monotonically as we move from the center of the trap toward the edges. For larger values of U (U>6) the density profile develops a well defined plateau at $\langle n_i\rangle$=1 and the length of the plateau grows as U is increased further. A simple way to

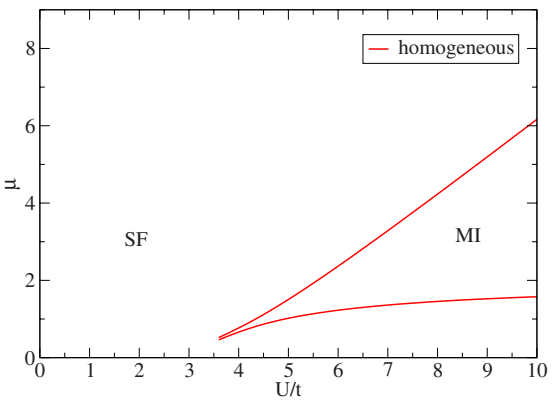

FIG. 2. (Color online) Phase diagram for the homogeneous Bose-Hubbard model. The MI phase has density ρ=1.

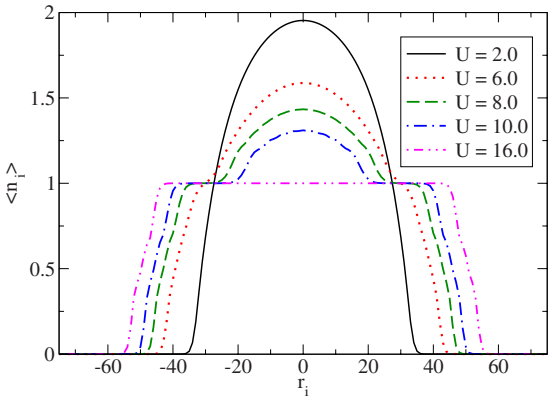

FIG. 3. (Color online) Density profile as a function of r_i for V_t=0.004 and N=100 for a range of U. Note that as the on-site repulsion increases, a MI phase forms around the central SF phase, finally leading to a central MI phase for higher values of U.

understand the behavior of $\langle n_i\rangle$ is through the local density approximation (LDA) [23,35] where the local density at site i in the trapped case is given by the density of a homogeneous system with a chemical potential

$$\mu_i = \mu - V_t r_i^2. \tag{8}$$

Here μ refers to the chemical potential at the center of the lattice where the trap potential is zero. Using Eq. (8) we can rescale the x axis of Fig. 3, so that we get the local density as a function of the local chemical potential, as shown in Fig. 4 for U=3 and 9, where the homogeneous case is also documented for comparison. Here we use a trap of depth V_t =0.004 with length L=200 and a trap of depth V_t=0.008 with length L=100. The number of bosons in the system are N=100 and 70 for V_t=0.004 and 0.008, respectively. The density profile as a function of the distance from the center of the lattice is shown in the inset. The local density as a

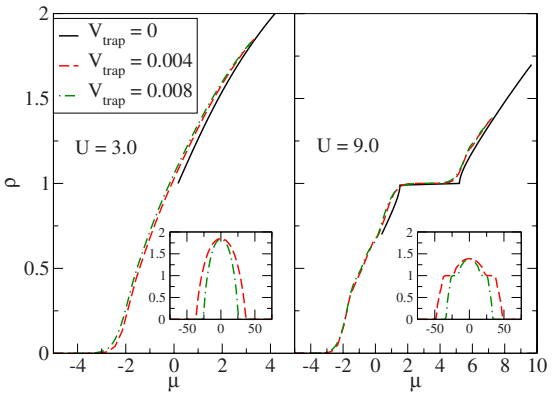

FIG. 4. (Color online) Density as a function of chemical potential for the homogeneous and inhomogeneous cases. The solid line represents the homogeneous system; the dashed lines and dashed-dotted lines represent the inhomogeneous case (V_t=0.004, N=100 and V_t=0.008, N=70, respectively). The inset shows the density profile as a function of the distance from the center of the trap. The homogeneous case has sharp transitions compared to the finite trap case.

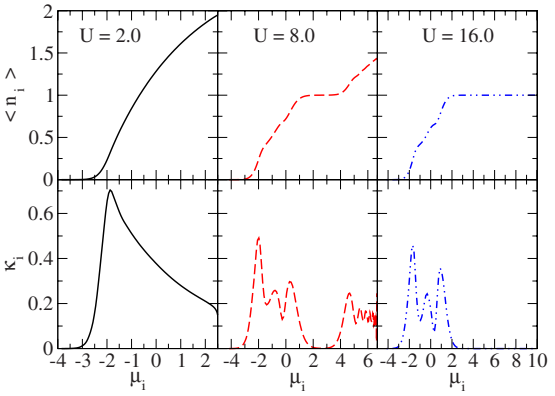

FIG. 5. (Color online) Local density and local compressibility as a function of the local chemical potential for $V_t=0.004$, $L=200$, and $N=100$.

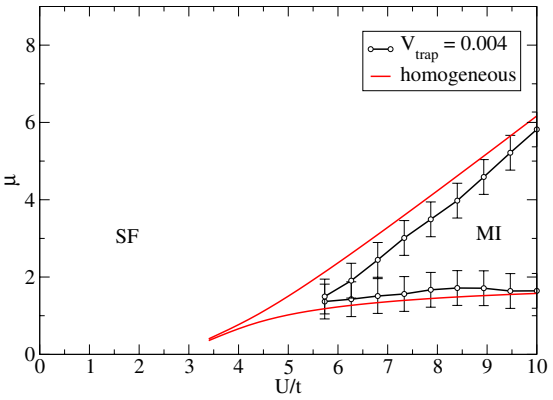

FIG. 6. (Color online) Homogeneous and inhomogeneous phase diagram. The error bars are obtained by varying the tolerance used to pick out the $\rho=1$ Mott plateau by 10%.

function of the local chemical potential exhibits trends similar to the homogeneous system; that is, the value of $\langle n_i \rangle$ increases smoothly as μ_i increases for lower values of U, where the entire system is in the compressible superfluid phase. However, as U increases further, a clear plateau emerges at $\langle n_i \rangle = 1$ indicating the onset of the $\rho=1$ MI phase.

The local compressibility can be obtained from the local density using Eq. (7). Figure 5 shows the local density and the local compressibility in the upper and the lower panels, respectively. The plateau region at $\langle n_i \rangle = 1$ (upper panels) has the corresponding local compressibility equal to zero. This verifies that the plateau present in the number density profile represents the MI phase. Furthermore, this confirms the coexistence of the SF and the MI phases in the presence of a trap. Though there is an overall agreement between the homogeneous and the inhomogeneous cases, we note that there are slight discrepancies. The sharp SF-MI transition observed in the homogeneous system is smoothened out in the presence of a trap. The cusplike behavior observed in κ for the homogeneous case is also lost. The agreement between the homogeneous and the inhomogeneous cases prompted us to obtain the phase diagram for the inhomogeneous system, by analogously picking out the values of μ at the knees where $\langle n_i \rangle = 1$, and plotting them in the μ-U plane. The resultant phase diagram is compared with the homogeneous result in Fig. 6. It is interesting to note that the MI lobe for the inhomogeneous system lies within that of the homogeneous system. However, the MI lobe retains its cusplike shape. Thus the SF-MI transition for density $\rho=1$ and $V_t>0$ does have the Kosterlitz-Thouless universality class behavior.

IV. EXPERIMENTAL SIGNATURES

In the earlier section we have established that the ground state phases for the Bose-Hubbard Hamiltonian given by Eq. (1) are either the superfluid or the Mott insulator depending on the ratio of U/t and the local chemical potential μ_i. Since μ_i is uniform for the homogeneous system, the ground state is global in nature. However, for inhomogeneous systems, μ_i being nonuniform, both the SF and the MI phases coexist, as already discussed. It would be worthwhile to explore the signatures of these coexisting phases in experimentally determined quantities.

It is now possible in experiments to record the spatial distribution of the lattice with different filling factors using spatially selective microwave transitions and spin-changing collisions as shown by Fölling *et al.* [27]. Similar experiments in one-dimensional optical lattices can yield density profiles from which the phase diagram can be obtained, as discussed in the previous section. Another way to obtain direct information about the Mott plateaus (shells in 3D) is through the atomic clock shift experiment [28]. By using density dependent transition frequency shifts, sites with different occupations can be spectroscopically distinguished, thus giving us the information about the number of sites with a given density ρ, defined as $N(\rho)$. In Fig. 7 we plot $N(\rho)$ versus ρ for several values of U for a system with $V_t=0.004$ and $N=100$. The peak in $N(\rho)$ at $\rho=1$ for $U>6.0$ is a direct signature of a well developed Mott insulator plateau in the inhomogeneous system. The size of this peak increases with U and is consistent with the increase in the length of the MI plateau as shown in the phase diagram (see Fig. 6). From $N(\rho)$ we obtain the following quantities: N_{MI}/N, the fraction of the number of bosons in the Mott plateau and N_{SF}/N, the

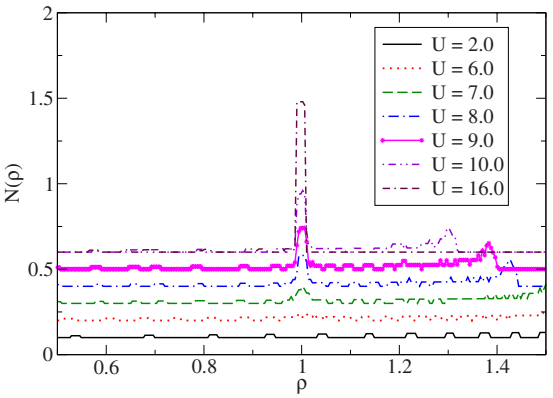

FIG. 7. (Color online) $N(\rho)$ versus ρ for $V_t=0.004$ and $N=100$. A small offset is added to the Y axis for clarity. The peak in $N(\rho)$ at $\rho=1$ signals the MI plateau in density profile (Fig. 3) and thus confirms the coexistence of SF and MI phases.

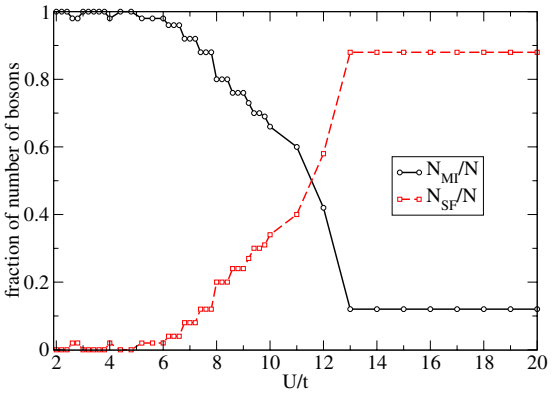

FIG. 8. (Color online) N_{MI}/N and N_{SF}/N as a function of U for $V_t=0.004$ and $N=100$. The critical on-site interaction $U_C\sim 6.0$ for the SF-MI transition for $\rho=1$ can be easily read off.

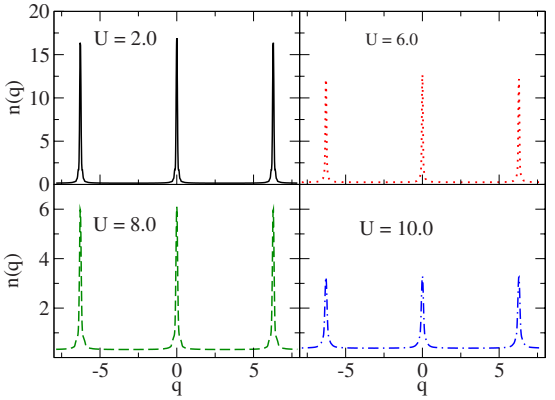

FIG. 9. (Color online) Momentum distribution as a function of q in units of the lattice spacing for a trap of $V_t=0.004$ and $N=100$. Note that at smaller U values there are three prominent interference peaks at $q=0$ and $q=\pm 2\pi$. As U increases, the peaks get smaller, indicating a transition from SF to MI.

fraction of bosons in the SF region. Here N_{MI} and N_{SF} are the number of bosons in the MI and the SF phases, respectively. Figure 8 shows both N_{MI}/N and N_{SF}/N for several values of U keeping $V_t=0.004$. For $U<6.0$, we observe that N_{SF}/N is close to one, while N_{MI}/N is close to zero. This is because the entire system is in the SF phase. However, for $U>6.0$, the increase in N_{MI}/N signals the formation of a MI plateau in the system. The critical value of U, marking the transition to the MI phase ($\rho=1$), can be read off from Fig. 8 and is given by $U_C\sim 6$. The small plateaus seen in N_{MI}/N and N_{SF}/N are indicative of the detailed distribution of the bosons as U increases in the presence of a trap. For $U\geqslant 13$, our inhomogeneous system has a central MI phase and the SF exist only at the edges. This is reflected in Fig. 8 where we see both N_{MI}/N and N_{SF}/N remain constant.

In other experiments, the cold atom gas trapped in an optical lattice is allowed to expand and the interference pattern in the density of the expanding gas is recorded. The density distribution is mirrored in the momentum distribution defined as

$$n(q)=\frac{1}{L}\sum_{k,l=1}^{L}\langle a_k^\dagger a_l\rangle \exp[iq(k-l)], \tag{9}$$

where k,l are the lattice sites. Figure 9 shows the momentum distribution for different U values. The superfluid phase that has long-range coherence exhibits sharp interference peaks, while the Mott-insulator phase, where the local density is pinned to integer values per site, breaks this coherence and hence no sharp peaks are observed [17]. Although the presence of the interference peaks in the density distribution (or analogously momentum distribution) was originally used to signal the formation of a SF phase, recently it has been established that the visibility of the interference fringes [29,38–40] provides a clear signature of the transition. The fringe visibility is defined as

$$\mathcal{V}=\frac{N_{\max}-N_{\min}}{N_{\max}+N_{\min}}, \tag{10}$$

where $N_{\max}$ and $N_{\min}$ are the maximum and the minimum of the momentum distribution measured at $q=\pm 2\pi$ and $q=\pm\pi$, respectively, in one dimension. The condensate fraction, that is, the number of bosons in the condensate with respect to the total number of bosons, is defined as the largest eigenvalue of the matrix $\langle a_i^\dagger a_j\rangle$ divided by the total number of bosons [42]. The fringe visibility and the corresponding condensate fraction for $V_t=0.004$, $N=100$ and $V_t=0.008$, $N=50$ are given in Figs. 10 and 11, respectively.

For a system in uniform SF phase, the fringe visibility is 1 [39]. In the homogeneous case, when the system undergoes a quantum phase transition from SF to MI, the visibility falls monotonously [29,41]. In the presence of a trap, however, the visibility as a function of U has a rich structure due to the formation of alternating SF and MI shells [38]. From Figs. 10 and 11, we note the following for the trap case: (1) the visibility remains finite even at high U values (i.e., deep inside the MI lobes) compared to the homogeneous case, (2) kinks develop over a certain range of U, and (3) the visibility drops drastically for particular values of U and for a further increase in U, the variation is slow. Similar behavior is also noted in the condensate fraction.

For a given value of U and number of bosons N, the homogeneous system is represented by a point (μ,U) in the

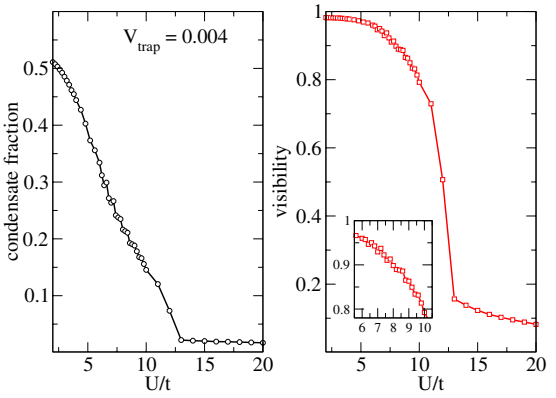

FIG. 10. (Color online) Condensate fraction (left) and visibility (right) as a function of U for a trap of depth $V_t=0.004$ and $N=100$. The inset zooms in on the kinks observed in the visibility corresponding to the formation of Mott shoulders.

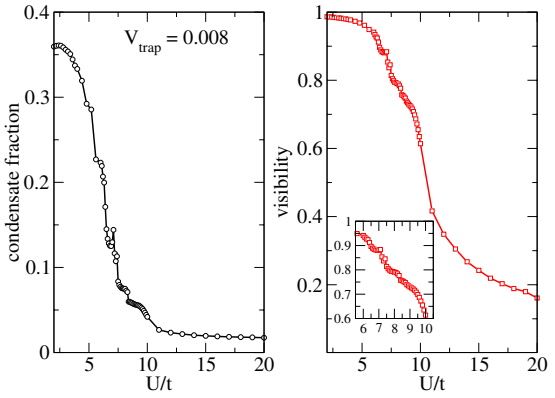

FIG. 11. (Color online) Condensate fraction (left) and visibility (right) as a function of U for a trap of depth V_t=0.008 and N=50.

phase diagram given in Fig. 6. However, for an inhomogeneous system the chemical potential varies across the lattice and is represented by a vertical line (see Fig. 12), originating at μ_0 for a given U in the (μ-U) plane, where μ_0 is the chemical potential at the center of the trap. The values of μ_0 as a function of U are shown in Fig. 12. The behavior of the condensate fraction and the visibility (shown in Figs. 10 and 11) are then easily understood by tracing the μ_0 trajectory as a function of U. For $U<6.0$, a vertical line starting at μ_0, representing possible values of the local chemical potential for a given U, does not intersect the MI lobe and no Mott plateau forms in the density profile. As U increases, the system begins to favor the MI phase, and as a result the condensate fraction and the visibility decreases monotonically. However, for $U>6.0$, the vertical line intersects the Mott lobe, resulting in a well-developed Mott plateau in the density profile. All the kinks in the condensate fraction and the visibility are observed for $U>6.0$, indicating the formation and broadening of the Mott plateau in the system, as the bosons redistribute themselves between the two phases across the lattice. Finally, for larger values of U, the μ_0 trajectory enters the Mott lobe and the central SF region vanishes completely. The entire system is in the Mott phase

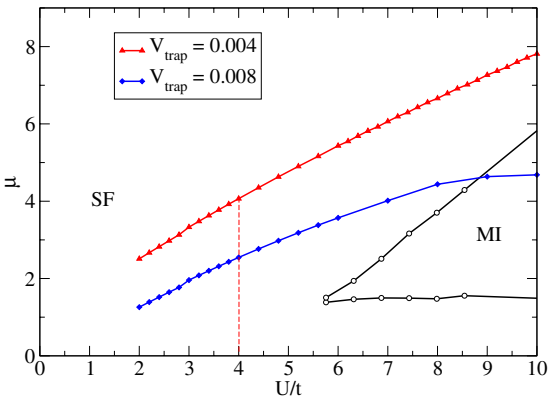

FIG. 12. (Color online) Variation of μ_0, the local chemical potential at the center of the trap, as a function of U. Here we use two sets of parameters: V_t=0.004, N=100 and V_t=0.008, N=50. For a given value of U, the inhomogeneous system can be represented by a vertical line originating at μ_0.

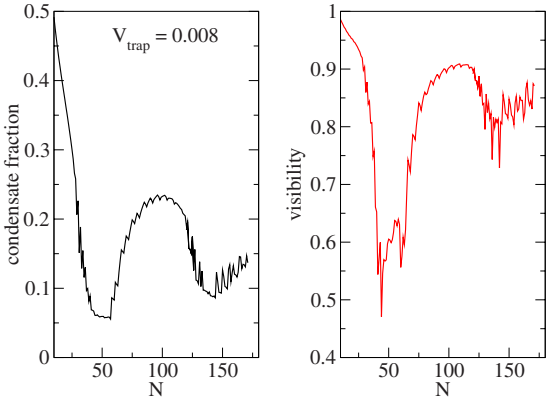

FIG. 13. (Color online) Condensate fraction (left) and visibility (right) as a function of N, the total number of bosons in a trap of depth V_t=0.008 and U=10. Both the condensate fraction and visibility show local minima for particular ranges of N, indicating the formation of MI phases. The subsequent increase in these quantities indicates the formation of SF phases.

except for the edges. As a result, the condensate fraction and the visibility drops drastically. Further increase in U results in smooth variations of both these quantities as the SF phases exist only at the edges and the number of bosons in the SF phases do not vary much as shown in Fig. 8.

In the experiments, the chemical potential is usually changed by changing the number of bosons N. We plot, in Fig. 13, the variation of the condensate fraction and the visibility as a function of N, for V_t=0.008 and U=10. We see that when the MI plateau forms, both the visibility and condensate fractions dip. The first of these correspond to the formation of a ρ=1 Mott plateau and occurs around $N\sim40$. This can be observed in the density profile (see Fig. 14). The plateau in Fig. 13, in the condensate fraction, indicates the range of N for which the center of the system has the ρ=1 MI phase for the given U value. We note that beyond $N\sim56$, a $1\leqslant\rho\leqslant2$ SF forms, marked by an increase in the visibility and the condensate fraction. The second minimum occurs around $N\sim140$ and signals the formation of the second Mott plateau (ρ=2), as shown in Fig. 14. A further increase in N, beyond $N\sim150$, results in another SF phase,

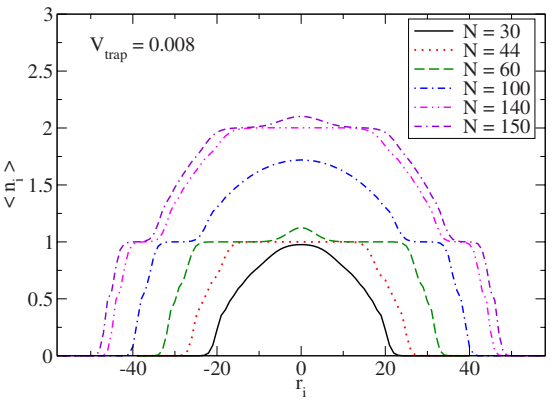

FIG. 14. (Color online) Density profile for a different total number of bosons N. Note that the minima in visibility and condensate fraction in Fig. 13 correspond to the formation of MI plateaus.

with the on-site density ranging between $2 \leqslant \rho \leqslant 3$. Therefore, for a fixed value of U, the minima in the condensate fraction and the visibility as a function of N are good indicators for the formation of Mott plateaus.

V. CONCLUSION

This paper demonstrates a way of extracting the phase diagram for the Bose-Hubbard model in the presence of a trap from the number density profile. Signatures of these phases in experimentally observed quantities such as visibility, condensate fraction, and $N(\rho)$ have been documented. We have also obtained the density profile as a function of the chemical potential for the homogeneous case, using FS-DMRG.

Future directions are immense. As a first step, the extended Bose-Hubbard model can be investigated and the phase diagram, together with the experimental signatures for the various phases, can be extracted in an analogous way, which is in progress. The influence of a three-body term for the Bose-Hubbard and the extended Bose-Hubbard can be investigated, which is also in progress.

The presence of a trap makes the system interesting due to the simultaneous existence of different phases (such as the SF and MI phase in this work) and gets the theoretical predictions closer to experiments. It would also be interesting to study the Bose-Hubbard model for two boson species and Bose-Fermi mixtures in the presence of a trap. This paper serves more as a benchmark to extract the phase diagram in a straightforward and transparent way from the density profile. This technique can now be extended to other problems.

ACKNOWLEDGMENTS

The computations were carried out on the Garuda grid and we thank its members for their support. M.L. thanks the Indian Institute of Astrophysics, Bangalore for their hospitality, where all of this work was carried out. R.V.P. thanks CSIR, India Grant No. 03(1107)/08/EMR-II.

[1] F. Dalfovo, S. Giorgini, L. P. Pitaevskii, and S. Stringari, Rev. Mod. Phys. **71**, 463 (1999).
[2] I. Bloch, J. Dalibard, and W. Zwerger, Rev. Mod. Phys. **80**, 885 (2008).
[3] M. Lewenstein, A. Sanpera, V. Ahufinger, B. Damski, A. Sen, and U. Sen, Adv. Phys. **56**, 243 (2007).
[4] M. P. A. Fisher, P. B. Weichmann, G. Grinstein, and D. S. Fisher, Phys. Rev. B **40**, 546 (1989).
[5] W. Krauth, M. Caffarel, and J. P. Bouchaud, Phys. Rev. B **45**, 3137 (1992).
[6] K. Sheshadri, H. R. Krishnamurthy, R. Pandit, and T. V. Ramakrishnan, Europhys. Lett. **22**, 257 (1993).
[7] L. Amico and V. Penna, Phys. Rev. Lett. **80**, 2189 (1998).
[8] T. D. Kuhner and H. Monien, Phys. Rev. B **58**, R14741 (1998); T. D. Kuhner, S. R. White, and H. Monien, *ibid.* **61**, 12474 (2000).
[9] R. V. Pai and R. Pandit, Phys. Rev. B **71**, 104508 (2005).
[10] R. V. Pai, R. Pandit, H. R. Krishnamurthy, and S. Ramasesha, Phys. Rev. Lett. **76**, 2937 (1996).
[11] V. A. Kashurnikov and B. V. Svistunov, Phys. Rev. B **53**, 11776 (1996).
[12] G. G. Batrouni, R. T. Scalettar, G. T. Zimanyi, and A. P. Kampf, Phys. Rev. Lett. **74**, 2527 (1995); P. Niyaz, R. T. Scalettar, C. Y. Fong, and G. G. Batrouni, Phys. Rev. B **44**, 7143 (1991).
[13] J. K. Freericks and H. Monien, Europhys. Lett. **26**, 545 (1994); Phys. Rev. B **53**, 2691 (1996).
[14] B. Capogrosso-Sansone, N. V. Prokofev, and B. V. Svistunov, Phys. Rev. B **75**, 134302 (2007).
[15] Barbara Capogrosso-Sansone, Sebnem Gunes Soyler, Nikolay Prokof'ev, and Boris Svistunov, Phys. Rev. A **77**, 015602 (2008).
[16] D. Jaksch, C. Bruder, J. I. Cirac, C. W. Gardiner, and P. Zoller, Phys. Rev. Lett. **81**, 3108 (1998).
[17] M. Greiner, O. Mandel, T. Esslinger, T. W. Haensch, and I. Bloch, Nature (London) **415**, 39 (2002).
[18] I. B. Spielman, W. D. Phillips, and J. V. Porto, Phys. Rev. Lett. **98**, 080404 (2007).
[19] T. Stöferle, H. Moritz, C. Schori, M. Köhl, and T. Esslinger, Phys. Rev. Lett. **92**, 130403 (2004).
[20] S. Wessel, F. Alet, M. Troyer, and G. G. Batrouni, Phys. Rev. A **70**, 053615 (2004).
[21] V. A. Kashurnikov, N. V. Prokofev, and B. V. Svistunov, Phys. Rev. A **66**, 031601 (2002).
[22] D. van Oosten, P. van der Straten, and H. T. Stoof, Phys. Rev. A **63**, 053601 (2001).
[23] S. Bergkvist, P. Henelius, and A. Rosengren, Phys. Rev. A **70**, 053601 (2004).
[24] Lode Pollet, Stefan Rombouts, Kris Heyde, and Jorge Dukelsky, Phys. Rev. A **69**, 043601 (2004).
[25] B. DeMarco, C. Lannert, S. Vishveshwara, and T.-C. Wei, Phys. Rev. A **71**, 063601 (2005).
[26] Kaushik Mitra, C. J. Williams, and C. A. R. Sá de Melo, Phys. Rev. A **77**, 033607 (2008).
[27] Simon Folling, Artur Widera, Torben Muller, Fabrice Gerbier, and Immanuel Bloch, Phys. Rev. Lett. **97**, 060403 (2006).
[28] G. K. Campbell, J. Mun, M. Boyd, P. Medley, A. E. Leanhardt, L. G. Marcassa, D. E. Pritchard, and W. Ketterle, Science **313**, 649 (2006).
[29] Fabrice Gerbier, Artur Widera, Simon Fölling, Olaf Mandel, Tatjana Gericke, and Immanuel Bloch, Phys. Rev. A **72**, 053606 (2005).
[30] J. M. Kosterlitz and D. J. Thouless, J. Phys. C **6**, 1181 (1973).
[31] Thierry Giamarchi, *Quantum Physics in One Dimension* (Clarendon Press, Oxford, 2004).
[32] G. G. Batrouni *et al.*, Phys. Rev. Lett. **89**, 117203 (2002).
[33] C. Kollath, U. Schollwöck, J. von Delft, and W. Zwerger, Phys. Rev. A **71**, 053606 (2005).
[34] Laura Urba *et al.*, J. Phys. B **39**, 5187 (2006).
[35] G. G. Batrouni, H. R. Krishnamurthy, K. W. Mahmud, V. G.

Rousseau, and R. T. Scalettar, Phys. Rev. A **78**, 023627 (2008).
[36] S. R. White, Phys. Rev. Lett. **69**, 2863 (1992); , Phys. Rev. B **48**, 10345 (1993).
[37] U. Schollwöck, Rev. Mod. Phys. **77**, 259 (2005).
[38] P. Sengupta, M. Rigol, G. G. Batrouni, P. J. H. Denteneer, and R. T. Scalettar, Phys. Rev. Lett. **95**, 220402 (2005).
[39] R. B. Diener, Q. Zhou, H. Zhai, and Tin-Lin Ho, Phys. Rev. Lett. **98**, 180404 (2007).
[40] Y. Kato, Q. Zhou, N. Kawashima, and N. Trivedi, Nat. Phys. **4**, 617 (2008).
[41] F. Gerbier, A. Widera, S. Fölling, O. Mandel, T. Gericke, and I. Bloch, Phys. Rev. Lett. **95**, 050404 (2005).
[42] A. J. Leggett, Rev. Mod. Phys. **73**, 307 (2001).